

Granular packings with moving side walls

James W. Landry* and Gary S. Grest

Sandia National Laboratories, Albuquerque, New Mexico 87185, USA

(Received 19 September 2003; published 16 March 2004)

The effects of movement of the side walls of a confined granular packing are studied by discrete element, molecular dynamics simulations. The dynamical evolution of the stress is studied as a function of wall movement both in the direction of gravity as well as opposite to it. For all wall velocities explored, the stress in the final state of the system after wall movement is fundamentally different from the original state obtained by pouring particles into the container and letting them settle under the influence of gravity. The original packing possesses a hydrostaticlike region at the top of the container which crosses over to a depth-independent stress. As the walls are moved in the direction opposite to gravity, the saturation stress first reaches a minimum value independent of the wall velocity, then increases to a steady-state value dependent on the wall velocity. After wall movement ceases and the packing reaches equilibrium, the stress profile fits the classic Janssen form for high wall velocities, while some deviations remain for low wall velocities. The wall movement greatly increases the number of particle-wall and particle-particle forces at the Coulomb criterion. Varying the wall velocity has only small effects on the particle structure of the final packing so long as the walls travel a similar distance.

DOI: 10.1103/PhysRevE.69.031303

PACS number(s): 45.70.Cc, 83.80.Fg, 45.70.Qj

I. INTRODUCTION

There has been a recent resurgence in interest in the formation and structure of granular packings in the physics community [1,2]. One particular facet of granular packings to receive attention recently is their stress profiles, both because of the industrial applications of silos [3], and because of new experimental techniques to measure effective stress in packings [4–6]. The first theoretical attempt to understand stress in a silo geometry dates back over 100 years to Janssen [7], who obtained a one-parameter form for the vertical stress in a silo. Several assumptions were made to arrive at this result. One was to treat the granular material as a continuous medium where a fraction κ of vertical stress is converted to horizontal stress. Another assumption was that the forces of friction between particles and walls are at the Coulomb failure criterion: $F_t = \mu_w F_n$, where F_t is the magnitude of the tangential friction force, F_n is the normal force at the wall, and μ_w is the coefficient of friction for particle-wall contacts. This assumption is also known as incipient failure. For a cylindrical container of radius R with static wall friction μ_w and granular pack of total height z_0 , the Janssen analysis predicts the vertical stress $\sigma_{zz}(z)$ at a height z as

$$\sigma_{zz}(z) = \rho g l \left[1 - \exp\left(-\frac{z_0 - z}{l}\right) \right], \quad (1)$$

where the decay length $l = R/2\kappa\mu_w$. κ represents the fraction of the weight carried by the side walls, ρ is the volumetric density, g is gravity, and z_0 is height of the top of the packing.

Numerous experiments have been carried out to verify this theory, but precise experiments are difficult. Recently, extremely well-controlled experiments on granular packings

have been done [4,6] that show a deviation from the ideal Janssen form, which we shall hereafter refer to as the Vanel-Clément form. This phenomenological form with one additional free parameter includes a hydrostaticlike region of linear dependence of pressure with depth (defined by the length a), followed by a region that conforms to the Janssen theory:

$$\begin{aligned} z_0 - z < a: \sigma_{zz}(z) &= \rho g (z_0 - z) \\ z_0 - z > a: \sigma_{zz}(z) &= \rho g \left(a + l \left[1 - \exp\left(-\frac{z_0 - z - a}{l}\right) \right] \right). \end{aligned} \quad (2)$$

This form was also found in extensive molecular dynamics simulations of granular packings in both two and three dimensions [8,9]. These packings were created both through pouring and sedimentation and then allowed to settle under the influence of gravity.

Many questions about stress in granular packings still remain unanswered. Even after a packing has been formed, it may be perturbed in many ways that radically change its stress profile and physical structure. Many studies have focused on tapping as a means to compress the packing and its logarithmic response time [10–13]. Another method to perturb a packing is to move the side walls [14–16]. The effect of this movement is not well understood and is the focus of this study.

Recently, experiments have been conducted on granular packings in cylindrical containers with movable side walls [14–16]. The experiments make use of a movable cylinder enclosing a granular packing supported by an independent base. These experiments find over a wide range of wall velocities good agreement with the Janssen form for the vertical stress after the system has relaxed following cessation of wall movement. This is in contrast to the earlier experiments on packings with fixed side walls [4,6]. Here we present large-scale three-dimensional (3D) discrete element, molecu-

*Electronic address: jwlandr@sandia.gov

lar dynamics simulations of granular packings in cylindrical containers (silos) with movable side walls. Our aim is to understand how the motion of the side wall modifies the stress profiles in granular packings and to compare our results with the recent experimental findings [14–16]. We analyze how wall movement and its cessation affect the stress profile of the packings. We also investigate in depth the effects of wall movement on the internal structure and particle positions of these packings, which cannot be easily measured experimentally. The behavior of the system under wall movement is similar across a wide range of wall velocities. Finally, we show that wall movement in the direction opposite to gravity drives tangential forces to the Coulomb criterion everywhere, leading directly to the Janssen form for the stress profiles.

The simulation technique and model are presented in Sec. II. The stress profiles and their features are discussed in Sec. III. In Sec. IV we examine the particle motion during and after wall movement, while in Sec. V we discuss the force distribution of the resultant packings. A brief summary and conclusions are presented in Sec. VI.

II. SIMULATION METHOD

We present discrete element, molecular dynamics (MD) simulations in 3D of model systems of $N=50\,000$ monodispersed spheres of fixed mass m and diameter d . The system is constrained by a cylinder of radius $R=10d$, centered on $x=y=0$, with its axis along the vertical z direction. The cylinder is bounded below by a layer of randomly-arranged immobilized particles approximately $2d$ high to provide a rough base. This work builds on previous MD simulations of packings in silos, where further details of the model can be found [8].

The spheres interact through a contact force model designed to include the major features of granular interactions. The main feature of the model is a spring-dashpot interaction in both the normal and tangential directions to the lines of the sphere centers. Contacting spheres i and j positioned at \mathbf{r}_i and \mathbf{r}_j experience a relative normal compression $\delta=|\mathbf{r}_{ij}-d|$, where $\mathbf{r}_{ij}=\mathbf{r}_i-\mathbf{r}_j$, which results in a force

$$\mathbf{F}_{ij}=\mathbf{F}_n+\mathbf{F}_t. \quad (3)$$

The normal and tangential contact forces are given by

$$\mathbf{F}_n=f(\delta/d)\left(k_n\delta\mathbf{n}_{ij}-\frac{m}{2}\gamma_n\mathbf{v}_n\right), \quad (4)$$

$$\mathbf{F}_t=f(\delta/d)\left(-k_t\Delta\mathbf{s}_t-\frac{m}{2}\gamma_t\mathbf{v}_t\right), \quad (5)$$

where $\mathbf{n}_{ij}=\mathbf{r}_{ij}/r_{ij}$, with $r_{ij}=|\mathbf{r}_{ij}|$. \mathbf{v}_n and \mathbf{v}_t are the normal and tangential components of the relative surface velocity, and $k_{n,t}$ and $\gamma_{n,t}$ are elastic and viscoelastic constants, respectively. $f(x)=1$ for Hookean (linear) contacts while for Hertzian contacts $f(x)=\sqrt{x}$. $\Delta\mathbf{s}_t$ is the elastic tangential displacement between spheres, obtained by integrating tangen-

tial relative velocities during elastic deformation for the lifetime of the contact. The magnitude of $\Delta\mathbf{s}_t$ is truncated as necessary to satisfy a local Coulomb yield criterion $F_t\leq\mu F_n$, where $F_t\equiv|\mathbf{F}_t|$ and $F_n\equiv|\mathbf{F}_n|$ and μ is the particle-particle friction coefficient. Frictionless spheres correspond to $\mu=0$. Contact surfaces are treated as “stuck” when $F_t<\mu F_n$ and as “slipping” when $F_t=\mu F_n$, which is known as the “proportional loading” approximation [17]. For this model, static and dynamic friction have the same μ . Particle-wall interactions are treated similarly, but the particle-wall friction coefficient μ_w is set independently. The side wall of the container is smooth, and thus the particle-wall normal force is always perpendicular to the xy plane. A more detailed description of the model is available elsewhere [8,18].

These simulations are run with a fixed set of parameters: $k_n=2\times 10^5 mg/d$, $k_t=\frac{2}{7}k_n$, and $\gamma_n=50\sqrt{g/d}$. For Hookean springs we set $\gamma_t=0$. In these simulations, it takes far longer to drain the energy out of granular packs using the Hertzian force law, since the coefficient of restitution ϵ is velocity-dependent [19] and goes to zero as the velocity goes to zero. We thus use Hookean contacts [20], which for the above parameters give $\epsilon=0.88$. The convenient time unit is $\tau=\sqrt{d/g}$, the time it takes a particle to fall its radius from rest under gravity. For this set of parameters, the time step $\delta t=10^{-4}\tau$. The particle-particle friction and particle-wall friction are the same: $\mu=\mu_w=0.5$. The simulations are run using a parallel distributed memory code on 20 DEC Alpha processors. One million time steps takes approximately 7 hours. Our longest simulation for slow wall velocities, $v=5\times 10^{-4}d/\tau$, ran for $t=1.14\times 10^4\tau$, which corresponds to approximately 800 h.

The simulations all begin with the same initial packing to minimize sample to sample fluctuations. This packing was generated by pouring particles into a container from a fixed height $Z=180d$. Particles are inserted over time and rain down to form the original packing, which then relaxes until it becomes quiescent [8]. Over the course of a simulation, the cylindrical side wall of the packing moves for a time t_s , which usually is $10^3\tau$, or over a fixed distance Δz . After this period, the walls cease to move and the packing settles. We consider a packing quiescent when the kinetic energy per particle $E_k\leq 10^{-8}mgd$. The time scale for this relaxation is very short, usually less than 10τ . The cylindrical side wall is moved either up ($+z$) or down ($-z$) with a constant velocity v_s varying from 10^{-1} to $10^{-5}d/\tau$. As in the experiments [14–16], only the side wall moves—the rough base is immobile throughout the course of the simulation.

The wall velocities used here for upward velocities are in the range used in the experiments by Bertho *et al.* [14]. In that study, glass beads with $d=2$ mm were moved with a velocity v_s ranging from 2×10^{-2} to 35 mm/s or 1.4×10^{-4} to $0.25d/\tau$ over distances up to $\Delta z=70$ mm = $35d$. Ovarlez *et al.* [15] use glass beads with $d=1.5$ mm and a fixed $v_s=1.5\times 10^{-3}$ mm/s or $1.2\times 10^{-5}d/\tau$ over a distance $\Delta z\approx 1.5\times 10^{-2}$ mm = $10^{-2}d$. This is a very low velocity over a very short distance. In an earlier study [6,4], Vanel *et al.* used a higher velocity, in conjunction with tapping, of $v_s=2\times 10^{-2}$ mm/s for particles of the same diameter. An-

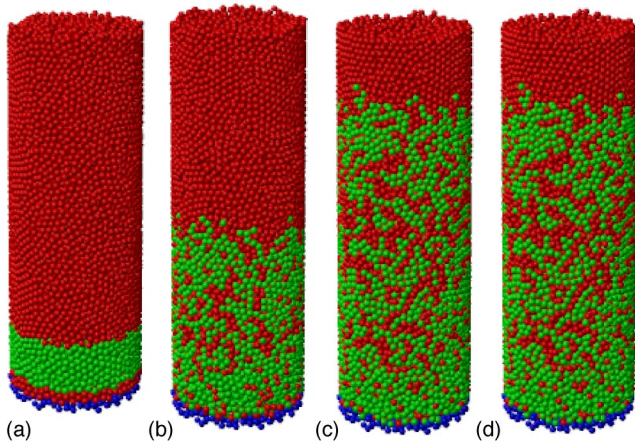


FIG. 1. (Color online) Effects of wall movement on an $N = 20\,000$ packing. The particles are shown in dark gray (red) and the fixed particles that form the base are shown in black (blue). All particles with initial positions between $z=5$ and $z=15$ have been colored light gray (green). The cylindrical wall is moved upwards ($+z$) with a velocity $v_s = 10^{-1}d/\tau$, a very high velocity. (a) The starting configuration before the wall moves. (b) The packing after the wall has moved for $5 \times 10^2\tau$, $\Delta z = 50d$. The packing is now taller—it has fluffed up as the wall has moved. Significant particle rearrangement is occurring. (c) The packing after the wall has moved for $10^3\tau$, $\Delta z = 100d$. Particles in contact with the wall have been dragged significantly up the pile. (d) The wall has stopped after $10^3\tau$ and the packing has reached equilibrium. There is little particle movement during relaxation.

other distinction between the experiments by Ovarlez *et al.* [15] and Vanel *et al.* [4,6] was the time at which measurement occurs. In the experiments of Ovarlez *et al.*, measurement occurs right at the end of wall movement, while in the experiments, of Vanel *et al.*, the packing is allowed to settle before measurements are made and tapping is sometimes also applied. Ovarlez and Clément also studied [16] moving the wall downwards with a v_s ranging from -5 nm/s to -100 $\mu\text{m/s}$, which corresponds to wall velocities of $-4 \times 10^{-8}d/\tau$ – $8 \times 10^{-3}d/\tau$. This range of velocities overlaps with our velocity range for downward wall movement, but also extends to much slower velocities.

Packings are examined both during wall movement and after cessation of wall movement and settling. Figure 1 shows the structure of a packing for a smaller system of 20 000 particles (used for illustration) with wall velocity $v_s = 10^{-1}d/\tau$ in the upward ($+z$) direction. This is a very high velocity, so during wall movement, there is significant particle rearrangement, and a number of particles originally in contact with the wall move upward. Particles between $z=5$ and $z=15$ have been colored light gray (green online) to provide a visual picture of particle movement over time. The height of the pile changes significantly during wall movement (4.7%), but does not change after the wall movement has ceased and the packing reaches equilibrium. For much slower wall velocities applied for the same time, very little particle movement is observed, and the height of the packing does not change.

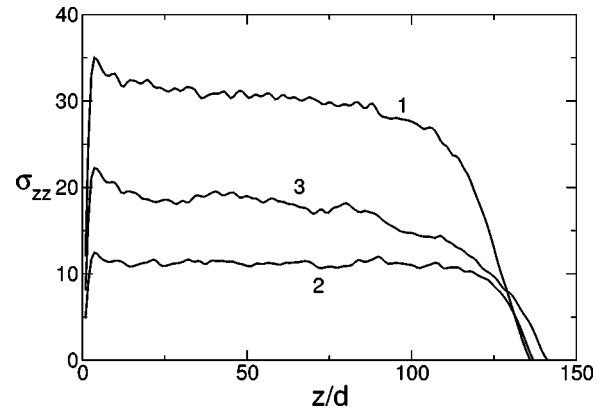


FIG. 2. Vertical stress σ_{zz} in units of mg/d^2 during wall movement with large velocity $v_s = 0.01d/\tau$. Profile 1 corresponds to the packing at $t=0$, the initial packing. Profile 2 is the same packing after the wall has moved for $t=100\tau$, a distance $\Delta z = d$. The saturation stress has fallen to $11mg/d^2$. Profile 3 is the same packing at $t=700\tau$ ($\Delta z = 7d$). The saturation stress first decreases to a minimum value and then increases to a steady state.

III. STRESS PROFILES

In this section we discuss the effect of wall movement on stress profiles of packings. In general, wall movement increases the tangential force between particles and the wall. The wall moves in relation to the particles, so the integrated displacement Δs increases as the wall moves. Since the tangential force is proportional to Δs , F_t increases over time. Wall movement thus drives F_t towards the Coulomb limit, $F_t = \mu_w F_n$, for particles in contact with the wall. We know from previous work [8] that the prime factor determining the form of the stress profile in these packings is the tangential force between particle and wall. If F_t is close to the Coulomb criterion, then we expect the stress to follow the Janssen form throughout the pile. In addition, the more particle-wall interactions that are at the Coulomb criterion, the stronger this effect and the lower the value of the saturation stress in the packing, i.e., the value of the stress in the depths of the packing, where the stress becomes depth-independent. We believe this effect is the origin of the experimental measurements observing remarkable agreement with the Janssen theory after the side walls of a packing are moved [14,15]. Below, we investigate the specific effects of wall movement on the stress profile.

Figure 2 shows the change in the stress profile of a packing with wall velocity $v_s = 0.01d/\tau$, a relatively large velocity. The stress profile with the largest saturation stress corresponds to $t=0$, before wall movement has begun. This stress profile obeys the Vanel-Clément form [4,8], with a linear stress profile at the top of the pile crossing over to a Janssen form in the depth of the pile. After moving the wall for $t=100\tau$, the saturation stress has decreased by more than a factor of three to $\sigma_{zz} \approx 11mg/d^2$ and the height of the pile has increased. As the wall movement continues, the saturation stress slowly increases. After a long time $t \geq 700\tau$, the system reaches steady state and the stress profile ceases to change markedly. Over the course of the wall movement, the height of the pile has increased by approximately 3%, and

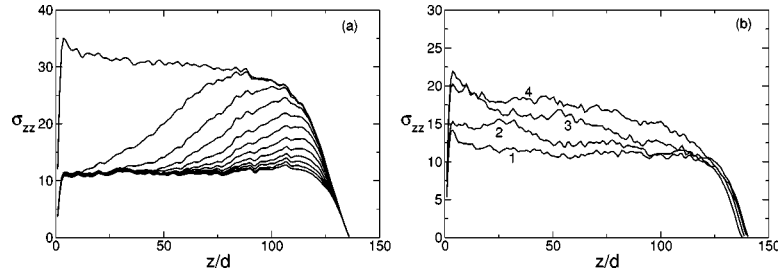


FIG. 3. Vertical stress σ_{zz} in units of mg/d^2 . (a) Stress progression for wall velocity $v_s = 10^{-4} d/\tau$. Here each stress profile is 200τ after the previous one, with the first profile corresponding to the packing before wall movement. The wall velocity is slow enough that the stress profile is only incrementally disrupted over time and does not attain the Janssen form until $t = 2200\tau$ and $\Delta z = 0.22d$. (b) Stress profiles for wall velocity $v_s = 5 \times 10^{-4} d/\tau$. Profile 1 is the minimum saturation stress $\sigma_{zz} \approx 11mg/d^2$ shown at $t = 2.8 \times 10^3 \tau$, $\Delta z = 1.6d$. Profile 2 is after $t = 6 \times 10^3 \tau$, $\Delta z = 3.1d$; profile 3 $t = 9 \times 10^3 \tau$, $\Delta z = 4.6d$; and profile 4 $t = 1.14 \times 10^4 \tau$, $\Delta z = 5.7d$. Over time the height of the packing as well as the saturation stress increase.

there has been considerable particle rearrangement. In addition, the linear stress disappears almost immediately after the initiation of wall movement. This change in the saturation stress is consistent with that observed in granular experiments performed by Bertho *et al.* [14], where the apparent mass (effectively the saturation stress) dropped quickly after the initiation of wall movement and then slowly increased with time until it reached a saturation value.

The behavior of the stress profile is similar for low wall velocities, although not identical. Unfortunately, computational limitations are much more severe for these packings than for high wall velocity packings, because the computational time required for the side wall to travel the same distance is so much larger. Figure 3(a) shows the change in the stress profile for a relatively slow wall velocity $v_s = 10^{-4} d/\tau$. Each profile is $2 \times 10^2 \tau$ after the previous one, starting at $t = 0$. For this wall velocity, the stress drops quickly at the base of the pile, but initially remains unchanged at the top of the pile. As wall movement continues, the new reduced stress profile propagates up the pile. Eventually, after moving the walls for $t = 2.2 \times 10^3 \tau$, which corresponds to a very small vertical distance $\Delta z = 0.22d$, the entire stress profile follows the Janssen form. At this point in the simulation, the height of the pile has not changed. This minimum saturation stress is the same as that observed in Figure 2, $\sigma_{zz} \approx 11 mg/d^2$, and is stable for a significant period of subsequent wall movement. This suggests that this is the limit for low saturation stress in this packing, and its value is controlled purely by geometric factors.

We explored the full behavior of the stress profile during wall movement using a low wall velocity of $v_s = 5 \times 10^{-4} d/\tau$ for $1.14 \times 10^4 \tau$, so that the side walls moved a total distance of $\Delta z = 5.7d$, which is comparable to the distance walls were moved for higher velocities. As shown in Fig. 3(b), prolonged wall movement at low velocities does eventually move the stress profile away from the minimum saturation stress. Prolonged wall movement also increases the height of the pile by 3.3%, which is similar to the height change for packings with high wall velocities. As the wall moves upward, changes in the stress profile propagate upwards from the bottom of the pack to the top. This occurs not only at early times, when the minimum saturation stress is propagated up the pile, but also at later times, when enhanced stress is also propagated up the pile as further wall movement increases the eventual saturation stress. This drop to a minimum saturation stress followed by an increase to a larger, stable saturation stress is the same for all observed wall velocities. The drop to a minimum saturation stress occurs at wall movement distances $\Delta z \approx 0.3d$ for all wall velocities measured. In addition, the increase in saturation stress from the minimum occurs when the wall has moved a distance $\Delta z \approx 1.6d$. At this distance, particles near the wall have completely moved past nearby particles, which means that whatever contacts these particles had initially have been destroyed. The minimum saturation stress is thus the optimized stress network for a given initial condition, and wall movement of greater than d destroys the initial stress network, and forms another, which is no longer optimal. This

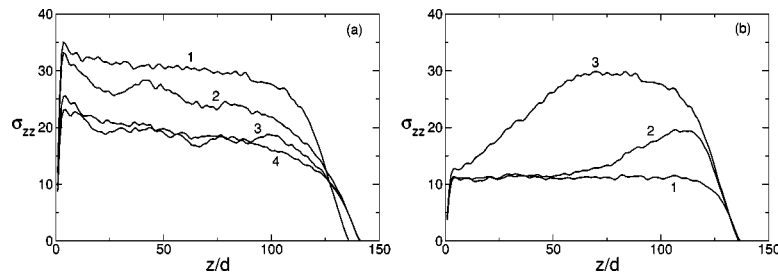


FIG. 4. Vertical stress σ_{zz} in units of mg/d^2 for packings moved for $t = 10^3 \tau$ and then allowed to relax. (a) High wall velocity profiles. Profile 1 corresponds to the initial packing. Profile 2 is the packing for $v_s = 10^{-1} d/\tau$, profile 3 $v_s = 10^{-2} d/\tau$, and profile 4 $v_s = 10^{-3} d/\tau$. (b) Low wall velocity profiles. Profile 1 corresponds to $v_s = 5 \times 10^{-4} d/\tau$, profile 2 to $v_s = 10^{-4} d/\tau$, and profile 3 to $v_s = 10^{-5} d/\tau$.

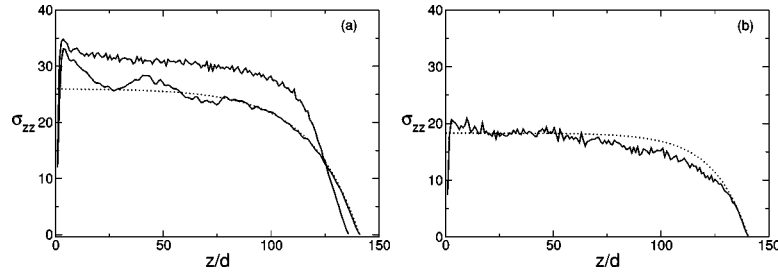


FIG. 5. Vertical stress σ_{zz} in units of mg/d^2 for a $N=50\,000$ particle packing. (a) Wall velocity $v_s=0.1d/\tau$ for $\Delta z=100d$ after cessation and relaxation compared to the original packing and (b) wall velocity $v_s=5\times 10^{-4}d/\tau$ for $\Delta z=5.7d$ after cessation and relaxation. The fit to the Janssen form is shown as a dotted line.

process is not steady, however. The stress changes relatively abruptly at certain times, then remains essentially unchanged for long periods (on order of $3\times 10^3\tau$ for $v_s=5\times 10^{-4}d/\tau$), then abruptly changes again. One exception to this is that the height of the packing increases smoothly with time until it reaches a stable height at $\sim 9\times 10^3\tau$ of $140.5d$, after which it remains unchanged under further wall movement.

Figure 4 shows the final stress profiles for the same packings after moving the wall for $t=10^3\tau$ for high and low wall velocity and then allowing them to settle. The wall movement has very different effects on the final stress profile depending on its strength. As seen in Fig. 4(a), wall velocities of $v_s\geq 10^{-3}d/\tau$ increase the height of the pile relative to the original packing, even after relaxation. The change in height is substantial and similar for many different wall velocities, 3.7%, meaning there has been a large change in the density of the packing. The final stress after relaxation is related to the magnitude of the velocity v_s , for $v_s\geq 10^{-3}d/\tau$. Those packings with larger v_s had larger saturation stress in the final packing. As we shall see in Sec. IV, the larger v_s , the more the particles rearrange. In addition, the larger v_s is, the larger the particle rearrangement after cessation of wall movement. This suggests that particle rearrangement strongly influences the final saturation stress. Those packings

with large v_s have enough particle rearrangement to completely disrupt the force network. The higher the velocity, the more contacts both at the wall and in the bulk are broken and the larger the eventual saturation stress. This behavior was also observed by Bertho *et al.* [14]: after the wall stopped moving, the packing settled and the apparent mass increased. In addition, they observed the same trend after relaxation. The larger the v_s , the larger the final saturation stress.

By contrast, small wall velocities ($v_s<10^{-3}d/\tau$) do not change the height of the pile over the same time period, largely because the wall does not travel far enough to substantially disrupt the force network. Large-scale rearrangements do not occur for this time duration. In this case, the particles against the wall are fully mobilized and the resultant saturation stress is small, because most of the pressure is supported by the walls. When the packing is allowed to relax, there are no large particle rearrangements, because the wall movement is not large enough to move particle positions significantly, and the wall movement has not put very much energy into the packing. The packing stays in the minimum saturation stress configuration. In addition, if the wall does not move for long enough to force the entire packing into the minimum saturation stress configuration, the intermediate stress configuration is stable under relaxation, as shown in Fig. 4(b) for the packing with wall velocity $v_s=10^{-4}d/\tau$.

If the walls are moved long enough at a low velocity to

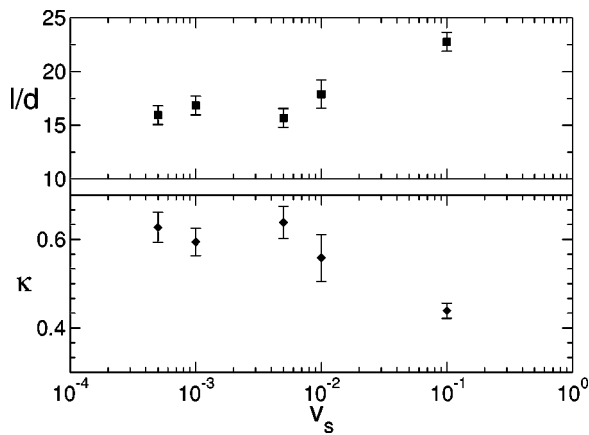


FIG. 6. Janssen length l and fraction of weight κ for different wall velocities after cessation of wall movement and relaxation. Fast wall velocities $v_s\geq 10^{-3}d/\tau$ were applied for $t=10^3\tau$, while the $v_s=5\times 10^{-4}d/\tau$ data were obtained after applying the wall velocity for $t=1.14\times 10^4\tau$.

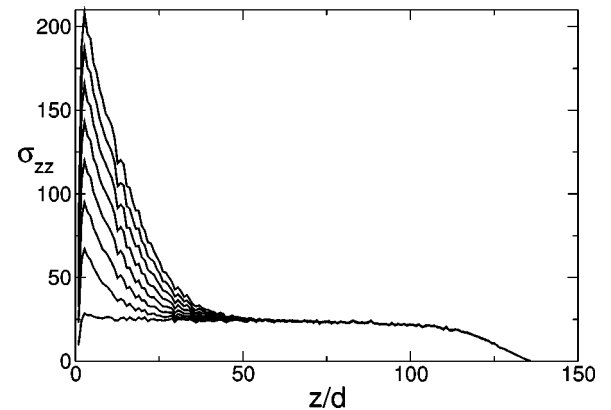


FIG. 7. Vertical stress σ_{zz} in units of mg/d^2 for a particle packing with wall velocity $v_s=-10^{-4}d/\tau$ starting at $t=0$ and every $10^2\tau$ afterward. The stress at the bottom of the packing increases with time. This stress does not dissipate after relaxation.

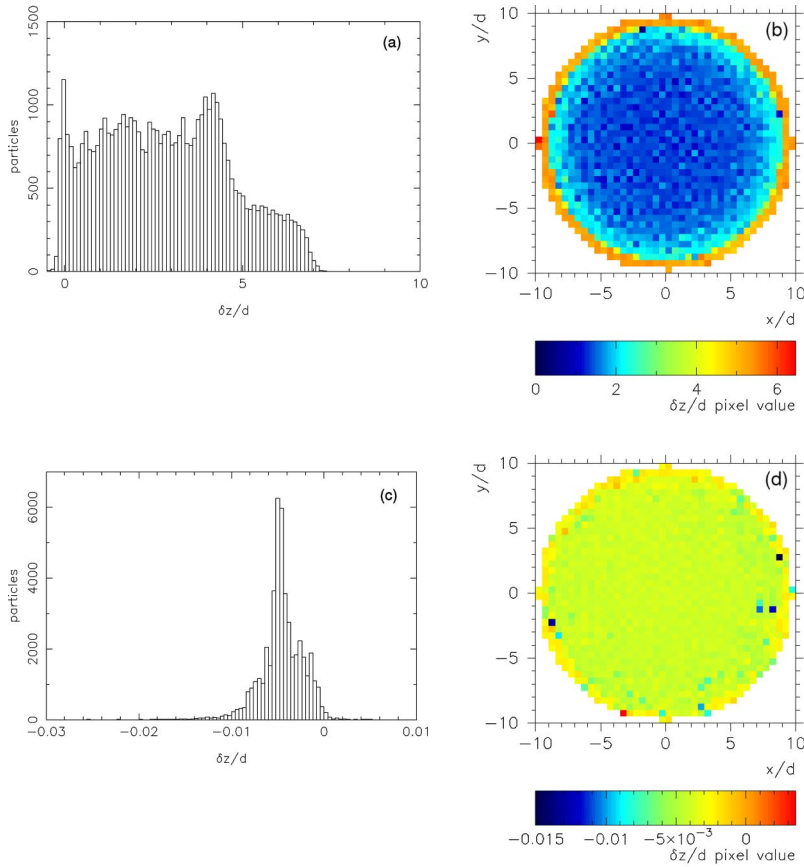


FIG. 8. (Color online) δz , distance traveled by particles in the z direction for $v_s = 10^{-2} d/\tau$. (a) Histogram of $\delta z/d$ starting from static packing and moving walls for $t = 10^3 \tau$. Particles have moved upward up to $7d$. (b) The same data averaged over z and presented as an image map. There is only a small region of rapid upwards movement near the wall. The bulk of the sample moves upward only slowly. The following two plots cover the changes in $\delta z/d$ after wall movement has ceased and the packing has settled. (c) Histogram of $\delta z/d$ from cessation of wall movement to a completely relaxed state. Particles settle, but not nearly as much as the particles traveled over the course of the wall movement. (d) Same image map as in (b). Here the particles settle more in the center than on the sides.

approach the stable final saturation stress (higher than the minimum saturation stress) the height of the pile does increase, as shown in Fig. 3(b) for $v_s = 5 \times 10^{-4} d/\tau$. After relaxation, however, the stress remains unchanged. The slow wall movement does not introduce enough energy into the packing for the stress to change during relaxation, even though for these long times, there is significant particle rearrangement before relaxation.

Figure 5 shows a comparison of the stress profile of two distinct packings. The first is the original quiescent packing. The second packing is this same packing after the wall has moved for $t = 10^3 \tau$ at $v_s = 0.1 d/\tau$ and then the packing has settled. The nature of the stress profile has been radically changed. While the original packing fits very well the Vanel-Clément form [4], the same packing after wall movement fits the one parameter Janssen form [7] well with $\kappa = 0.44$. As we shall see in Sec. V, the wall movement has forced the tangential force of the particles at the wall to the Coulomb criteria everywhere, eliminating the linear stress region. Another example is given for a slow velocity $v_s = 5 \times 10^{-4} d/\tau$, where $\kappa = 0.63$. In this case, however, the Janssen fit overshoots the actual stress near the top of the pack, the opposite of the case where it fails for the original stress

region. For all velocities observed, the linear stress region is destroyed, but only the high velocity cases fit the Janssen stress form well.

We have compiled κ 's for the various wall movement rates and show them in Fig. 6. These values can be compared with Fig. 4 in Bertho *et al.* [14]. In both cases, as the wall velocity increases, the resultant Janssen length l increases. Since $\kappa = R/2\mu_w l$, κ decreases with increasing wall velocity v_s . The κ 's observed are much lower than those obtained for the original packings with the Vanel-Clément form, which were slightly greater than 1 [8]. In our case, the intermediate stresses between the minimal stress and final stress do not follow the Janssen form and κ for those stress profiles has no meaning. Using the observed l and $R = 7.5d$ given in Ref. [14], we find κ 's ranging from $\kappa = 0.349$ for $v_s = 20 \text{ mm/s} = 0.14 d/\tau$ to $\kappa = 0.405$ for $v_s = 0.2 \text{ mm/s} = 1.4 \times 10^{-3} d/\tau$. These values are slightly lower but close to our observed values, shown in Fig. 6.

Downward motion of the wall is a very different phenomenon. In this case, the wall movement merely increases the stress at the base of the pile, without changing the stress profile elsewhere, as shown in Fig. 7, which shows the stress profile for a particle packing with $v_s = -10^4 d/\tau$ applied for

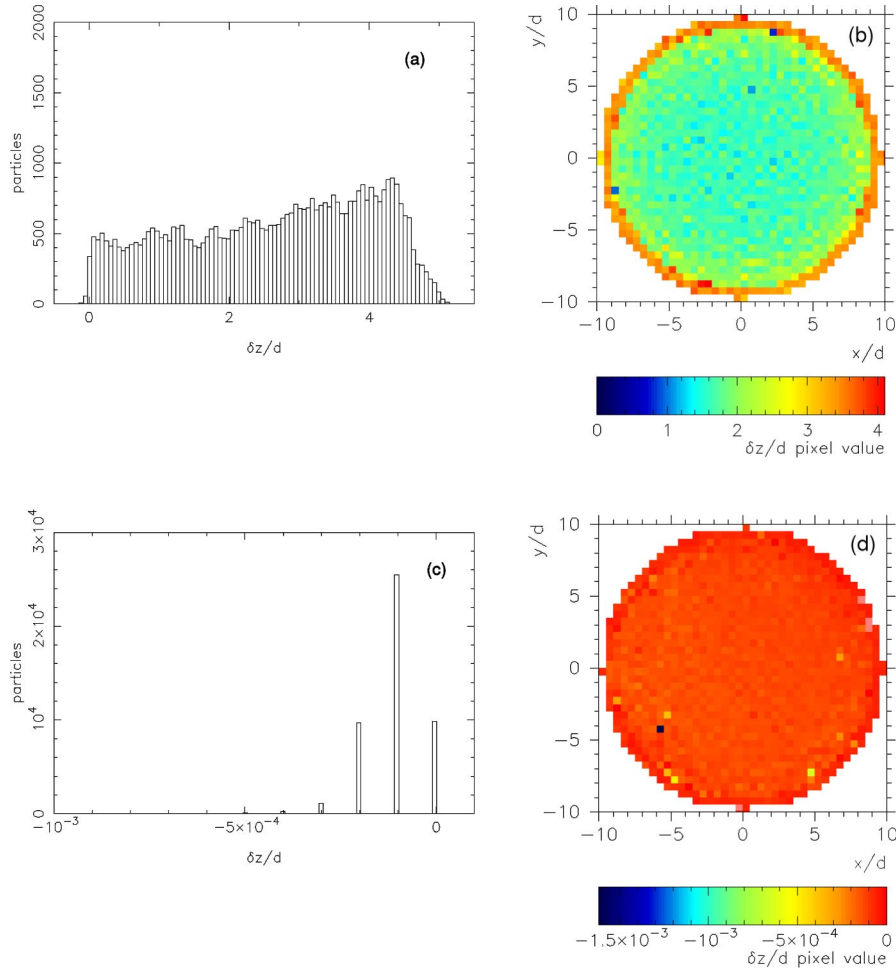


FIG. 9. (Color online) δz , distance traveled by particles in the z direction over time for $v_s = 5 \times 10^{-4} d/\tau$. (a) Histogram of $\delta z/d$ starting from static piles and moving walls for $t = 1.14 \times 10^4 \tau$. Particles have moved up more than $5d$ as the walls have moved $\Delta z = 5.7d$. (b) The same data averaged over z and presented as an image map. There is only a small layer of rapid upwards movement. The bulk of the sample moves upward only slowly. (c) Histogram of $\delta z/d$ from cessation of wall movement to a completely relaxed state. Particles settle, but not nearly as much as the particles traveled over the course of the wall movement. (d) Same image map as in (b). Here the particles settle more in the center than on the sides, though the difference is not as great as in the high velocity case.

$t_s = 10^3 \tau$. This stress buildup increases with duration of wall movement and occurs for all the velocities probed, from $v_s = -10^{-1} d/\tau$ to $-10^{-5} d/\tau$. In addition, this stress buildup is robust and does not disappear when the packing settles after cessation of wall movement. The extra stress is locked in. There is a slight difference between high and low wall velocities. Low wall velocities do not change the height of the packing, while high wall velocities ($v_s \geq 10^{-3} d/\tau$) increase the density at the bottom of the pile and lower the overall height of the packing by a slight amount.

IV. PARTICLE REARRANGEMENT

We have studied the motion of particles during and after wall movement to understand the effects of wall movement on the position and density of the packing. As the walls are moved upward with velocity v_s , they drag particles in contact with the walls upwards by means of the frictional force between them. As particles on the edge of the cylindrical container move upward, particles in the middle of the pack-

ing move downward and outward toward the walls to fill the voids created by the upward-moving particles.

We present two sets of data for both high and low velocities. The first data set is for a high wall velocity of $v_s = 10^{-2} d/\tau$, and is presented in two ways. The first is a histogram of the motion of the particles in z from their initial starting position to the final position after wall movement for $t = 10^3 \tau$, $\Delta z = 10d$. The measured movement of the particles in the z direction δz is recorded and a histogram is generated. Only those particles with an initial position $z \geq 10d$ are included. In the second method we average δz over z and present an image map of the motion of these particles in z . Both the top ($z > 120d$) and bottom ($z < 10d$) regions of the initial packing are excluded to avoid edge effects. These data sets are presented for the packing after wall movement for $t = 10^3 \tau$ and then after a relaxation to equilibrium in Fig. 8.

For high wall velocities, there is significant particle movement. In this case, particles travel upwards as much as $7d$. However, all of this movement is restricted to a small ring

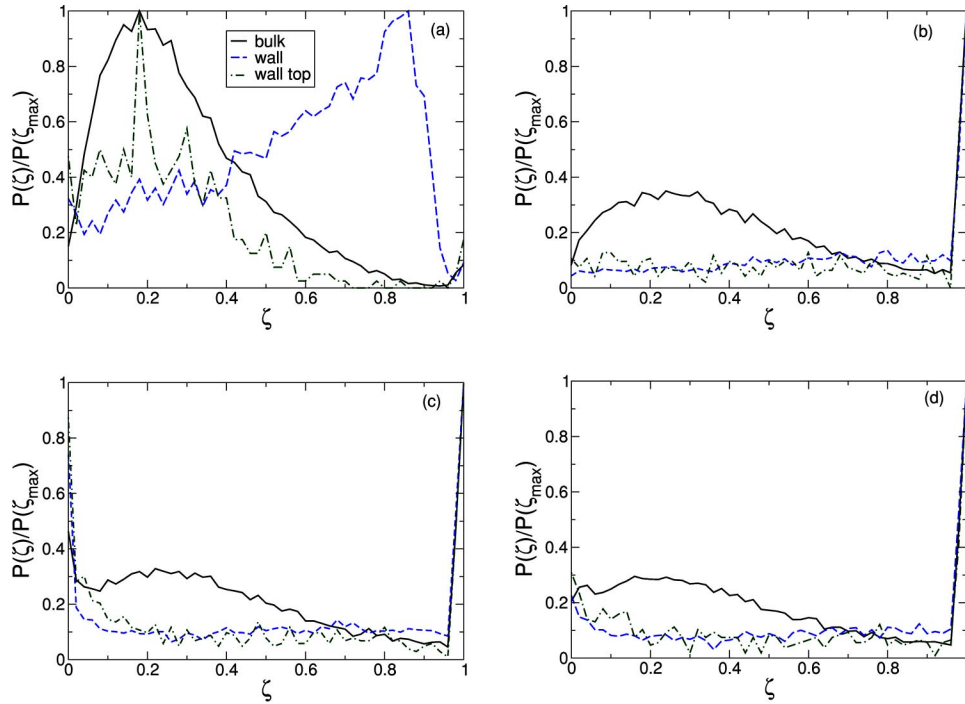


FIG. 10. (Color online) Ratio of normal forces to tangential forces in packings. The force distributions were analyzed in three different locations: bulk—in the depths of the packing away from the walls (solid line), wall—only the particle-wall interactions in the center of the pile (dashed line), and wall top—only the particle-wall interactions near the top of the pile (dot-dashed line). $\zeta = F_t / \mu F_n$ in the case of the bulk, $\zeta = F_t / \mu_w F_n$ otherwise. (a) Original quiescent packing. (b) After $v_s = 10^{-2} d/\tau$ for $t = 10^3 \tau$, $\Delta z = 5d$. (c) Same as in (b) after cessation of wall movement and relaxation (d) After $v_s = 5 \times 10^{-4} d/\tau$ for $t = 10^5 \tau$, $\Delta z = 5d$.

around the cylinder walls. In the center of the pack, particle movement is less than d . Particles slide past one another and the initial stress networks are quickly destroyed. New force networks are constantly created and destroyed over the course of the wall movement. It is relatively easy for particles to move past each other in the vertical direction, while horizontal motion is more difficult. This effect is also observed in vertically shaken granular materials [21,22]

The initial drop in the saturation stress when the side wall has moved approximately $0.3d$ is not enough to move the particles past each other. This minimum saturation stress thus reflects a particle configuration where the initial contacts have been strengthened. Once particles at the wall move past their original contacts, the original stress network is completely disrupted, and later networks as they form and dissolve support less stress, causing the saturation stress to increase.

When the wall movement stops, the packing settles, and the new δz is much smaller in magnitude than the δz during wall movement. Also, the particles at the wall move much less than the particles in the center, which suggests that the particles at the wall are supported by friction at the walls.

Figure 9 shows δz for the low wall velocity $v_s = 5 \times 10^{-4} d/\tau$ applied for the much longer time $t = 1.14 \times 10^4 \tau$ for a total wall movement of $\Delta z = 5.7d$. The change in particle heights for δz is similar to that seen in high velocity runs. Particles along the walls move upward much more than those in the center. However, unlike in the high-velocity case, there is no second ring of particles one or two d in from the wall that also shows a large δz relative to the center. In

this case, the particles not in contact with the wall show much less difference in δz as a function of radius.

Relaxation is very interesting in this case. The difference in δz between particles at the wall and particles in the bulk is much less than in the high velocity case. In addition, relaxation occurs in discrete jumps with many particles moving together. This is a general feature of δz relaxation histograms for low wall velocity packings. In the low velocity case, energy is imparted into the system very slowly and is dissipated more quickly. There is thus much less energy available to rearrange the packing after the wall movement ceases, and the relaxation of the particles is much less. In addition, because individual particles have very little kinetic energy when the wall movement ceases, motion happens coherently as many particles rearrange at once. This behavior is also seen in vibrated powders [21,22], where for low intensity vibrations, collective motion predominates, while for high intensity vibrations, particles move much more independently.

V. COULOMB CRITERION

We also examined the force distributions in the packings during and after wall movement. These provide further evidence that the final packing state after relaxation is very different from the initial state, and also demonstrate the different behavior of the two regimes after relaxation. A useful quantity is the ratio of normal forces F_n to tangential forces F_t . A key assumption of the Janssen analysis is that the ratio of these forces $\zeta = F_t / \mu_w F_n = 1$ for particle-wall forces in

the packing. These distributions are shown in Fig. 10 for several different packings. We consider three different distributions: forces in the bulk of the sample far from the wall, particle-wall forces in center of the packing, and particle-wall forces at the top of the packing. In this case, $\zeta = F_t/\mu F_n$ in the bulk of the sample, and $\zeta = F_t/\mu_w F_n$ for particle-wall forces.

The original packing has a strong peak near $\zeta=0.2$ in the bulk of the material, showing that the vast majority of forces are far from the Coulomb criterion. At the wall, the peak in the distribution is much closer to the Coulomb criterion at $\zeta\sim 0.9$. At the top of the packing, in the hydrostatic region [8], the distribution of forces is far from the Coulomb criterion.

After wall movement, the distribution of forces is radically changed. For both the high velocity ($v_s=10^{-2}d/\tau$) and low velocity ($v_s=5\times 10^{-4}d/\tau$) cases, all three distributions are driven toward the Coulomb criterion, with the peak in the distributions at the Coulomb criterion. In both cases, the original distribution is not completely destroyed. For the bulk distribution, a subsidiary peak appears in the new bulk distribution where the original peak appeared. This change in the distribution of forces is the main cause for the more Janssen-like stress distributions observed.

We also present results for the $v_s=10^{-2}d/\tau$ case after cessation of wall movement and relaxation in Fig. 10(c). In this case, the main change in the distribution after relaxation is the increase in particles forces at very low ζ . This occurs because some contacts between particles disappear during relaxation as particles move relative to their neighbors. When new contacts are made, these are far from the Coulomb criterion by definition, since particles are not, in general, rotating relative to each other during relaxation. By contrast, the low velocity case $v_s=5\times 10^{-4}d/\tau$. Figure 10 exhibits no change in the distribution of forces after cessa-

tion and relaxation. In this case, particles move together, and contacts are not destroyed or created, so the force distribution does not change. This lack of change in the force distribution may explain why low velocity packings do not exhibit perfect agreement with the Janssen form after relaxation.

VI. CONCLUSIONS

We have explored the effects of side wall movement on granular packings. Much of the resultant structure of the pack does not depend strongly on the magnitude of the wall movement, as long as the packing is moved for an equivalent distance. Small differences emerge in the behavior after cessation, where high wall velocity packings substantially rearrange and increase their saturation stress while low wall velocity packings remain essentially unchanged. The main effect of wall movement is to drive both the particle-wall and particle-particle contacts to the Coulomb criterion, so that the ratio of tangential forces to normal forces is maximized. This condition forces the packing in the high wall velocity case to obey the Janssen form, which takes the Coulomb criterion as one of its main assumptions. For low wall velocities, the final form is very different from the initial form, though it does not perfectly match the Janssen form.

ACKNOWLEDGMENTS

This work was supported by the Division of Materials Science and Engineering, Basic Energy Sciences, Office of Science, U.S. Department of Energy. This collaboration was performed under the auspices of the DOE Center of Excellence for the Synthesis and Processing of Advanced Materials. Sandia is a multiprogram laboratory operated by Sandia Corporation, a Lockheed Martin Company, for the United States Department of Energy's National Nuclear Security Administration under Contract No. DE-AC04-94AL85000.

-
- [1] H.M. Jaeger, S.R. Nagel, and R.P. Behringer, *Rev. Mod. Phys.* **68**, 1259 (1996).
 - [2] J. Duran, *Sands, Powders, and Grains: An Introduction to the Physics of Granular Materials* (Springer-Verlag, Berlin, 2000).
 - [3] R.M. Nedderman, *Statics and Kinematics of Granular Materials* (Cambridge University Press, Cambridge, 1992).
 - [4] L. Vanel and E. Clément, *Eur. Phys. J. B* **11**, 525 (1999).
 - [5] D.M. Mueth, H.M. Jaeger, and S.R. Nagel, *Phys. Rev. E* **57**, 3164 (1998).
 - [6] L. Vanel, P. Claudin, J.-P. Bouchaud, M. Cates, E. Clément, and J.P. Wittmer, *Phys. Rev. Lett.* **84**, 1439 (2000).
 - [7] H.A. Janssen, *Z. Ver. Dt. Ing.* **39**, 1045 (1895).
 - [8] J.W. Landry, G.S. Grest, L.E. Silbert, and S.J. Plimpton, *Phys. Rev. E* **67**, 041303 (2003).
 - [9] J.W. Landry, G.S. Grest, and S.J. Plimpton, *Powder Technol.* **139**, 233 (2004).
 - [10] J.B. Knight, C.G. Fandrich, C.N. Lau, H.M. Jaeger, and S.R. Nagel, *Phys. Rev. E* **51**, 3957 (2003).
 - [11] E.R. Nowak, J.B. Knight, E. Ben-Naim, H.M. Jaeger, and S.R. Nagel, *Phys. Rev. E* **57**, 1971 (1998).
 - [12] C. Josserand, A.V. Tkachenko, D.M. Mueth, and H.M. Jaeger, *Phys. Rev. Lett.* **85**, 3632 (2000).
 - [13] P. Philippe and D. Bideau, *Europhys. Lett.* **60**, 677 (2002).
 - [14] Y. Bertho, F. Giorgiutti-Dauphiné, and J.-P. Hulin, *Phys. Rev. Lett.* **90**, 144301 (2002).
 - [15] G. Ovarlez, C. Fond, and E. Clément, *Phys. Rev. E* **67**, 060302 (2003).
 - [16] G. Ovarlez and E. Clément, *Phys. Rev. E* **68**, 031302 (2003).
 - [17] T.C. Halsey and D. Ertas, *Phys. Rev. Lett.* **83**, 5007 (1999).
 - [18] L.E. Silbert, D. Ertas, G.S. Grest, T.C. Halsey, D. Levine, and S.J. Plimpton, *Phys. Rev. E* **64**, 051302 (2001).
 - [19] J. Schäfer, S. Dippel, and D.E. Wolf, *J. Phys. I* **6**, 5 (1996).
 - [20] We have made a packing using Hertzian springs and analyzed its behavior under wall movement and found no substantial difference in its behavior relative to that presented here.
 - [21] G.C. Barker and A. Mehta, *Phys. Rev. A* **45**, 3435 (1992).
 - [22] G.C. Barker and A. Mehta, *Phase Transitions* **75**, 519 (2002).